THE JOURNAL OF PHYSICAL CHEMISTRY B

Article

pubs.acs.org/JPCB

Impact of Ionic Liquid-Modified Multiwalled Carbon Nanotubes on the Crystallization Behavior of Poly(vinylidene fluoride)

Chenyang Xing, Liping Zhao, Jichun You, Wenyong Dong, Xiaojun Cao, and Yongjin Li*

College of Material, Chemistry and Chemical Engineering, Hangzhou Normal University, No. 16 Xuelin Road, Hangzhou 310036, China

Supporting Information

ABSTRACT: The impact of pristine multiwalled carbon nanotubes (MWCNTs), an ionic liquid (IL), 1-butyl-3-methylimidazolium hexafluorophosphate [BMIM][PF_6], and the ionic liquid-modified MWCNTs (IL-MWCNTs) on the crystallization behavior of melt-crystallized poly(vinylidene fluoride) (PVDF) has been investigated. Pristine MWCNTs accelerate crystallization of PVDF as an efficient nucleation agent, while the formed crystals are mainly nonpolar α crystal form with few polar β crystals. Incorporation of only ionic liquid results in depression of the PVDF melt crystallization rate due to the miscibility of IL with PVDF but leads to a higher content of polar crystals (β and γ forms) than MWCNTs. The ionic liquid and MWCNTs show significant synergetic effects on both the nucleation and the formation of polar crystals for PVDF by melt crystallization. Addition of IL-MWCNTs not only improves the MWCNTs dispersion in PVDF matrix but also increases the overall crystallization rate of PVDF drastically. More important, the melt-crystallized PVDF nanocomposites with IL-MWCNTs show 100% polar polymorphs but no α crystal forms. To the best of our knowledge, this is the first report on the achievements of full polar crystal form in the melt-crystallized PVDF without mechanical deformation or electric field. The IL to MWCNTs ratio and the IL-MWCNTs loading content effects on the crystallization behavior of PVDF in the nanocomposites were also studied. It is considered that the specific interactions between >CF_2 with the planar cationic imidazolium ring wrapped on the MWCNTs surface lead to the full zigzag conformations of PVDF; thus, nucleation in polar crystals (β and γ forms) lattice is achieved and full polar crystals are obtained by subsequent crystal growth from the nuclei.

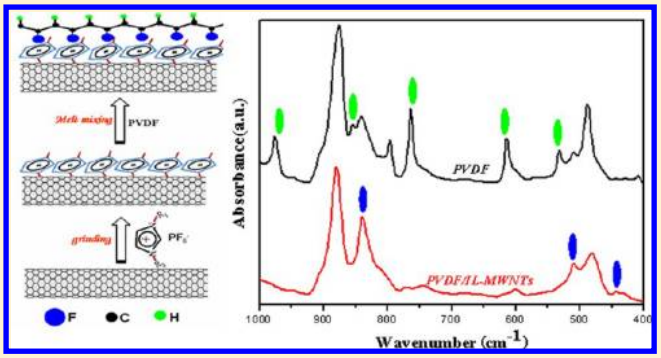

1. INTRODUCTION

In recent years polymer/carbon nanotubes (CNTs) nanocomposites have drawn considerable research interest because of their dramatic improvement in physical, thermal, mechanical, electrical, and electroactive properties compared to those in the pristine polymer. Although numerous investigations have been carried out to improve the compatibility between carbon nanotubes and polymer matrix, the homogeneous dispersion of CNTs in polymer matrices still presents significant challenges, especially for large-scale industrial applications. Noncovalent functionalization of nanotubes with appropriate treatment is an attractive strategy because it does not disrupt the extended π-conjugation structure and does not damage both the mechanical and the electrical properties of CNTs. Recently, ionic liquids (ILs) have been found to have strong "π-cation" interactions with CNTs,[1−3] which provides new possibilities to fabricate noncovalent modified carbon nanotubes for further dispersion in polymers. However, few studies have succeeded in dispersing IL-modified CNTs in polymer matrices so far.[4−7] In the present study, we modified the multiwalled carbon nanotubes (MWCNTs) with a widely used room-temperature ionic liquid, 1-butyl-3-methylimidazolium hexafluorophosphate [BMIM][PF_6], which renders the MWCNTs homogeneously dispersed in poly(vinylidene fluoride) (PVDF) matrix.

Poly(vinylidene fluoride) (PVDF) is an important polymer, and it has been extensively studied for its valuable application as piezoelectric and pyroelectric materials.[8] PVDF exhibits polymorphism of several crystalline phases and shows at least five possible types of crystal phase, so-called nonpolar α-phase, polar β-phase, and γ-, δ-, and ε-phase.[9] The most common polymorph of PVDF is α-phase having a monoclinic unit cell with *TGTG′* chain conformation. The α-phase is generally produced during crystallization from the melt. The β-phase and γ-phase are more attractive and desirable crystal types in PVDF as polar crystal forms and correspond to conformational sequences of TTTT and TTTG, respectively. The fluorine atoms are fully or dominantly located on the one side of the polymer chains,[10] which accordingly provides PVDF with much higher polarity compared with nonpolar α PVDF phase. The

Received: April 30, 2012
Revised: June 9, 2012
Published: June 18, 2012

dx.doi.org/10.1021/jp304166t | *J. Phys. Chem. B* 2012, 116, 8312−8320

polar phases, especially β-phase, exhibit excellent piezo- and pyroelectric properties as well as ferroelectric activity.

A variety of experimental techniques have been developed to induce \ formation of polar phases. The uniaxially stretching at appropriate temperature renders transformation of the helix conformation to the zigzag conformation of PVDF chains; thus, a high content of polar β-PVDF can be obtained.[10−13] Using this method one can seldom get complete nonpolar to polar phase transition and about 20% of α-PVDF will remain, depending on the drawing temperature and stretch ratio.[10,13] Solvent casting or crystallization from its solution in polar solvents was also used to fabricate the β-phase and γ-phase PVDF.[14,15] Different crystal phases exist in PVDF depending on preparation conditions like solvent, method of casting, stretching of thin films, and annealing conditions.

Nanofillers have been the focus recently as a means of enhancing polar phase crystals formation in PVDF. It has been found that nanoclay influences the PVDF structure, particularly β-phase crystal formation is enhanced.[16−20] However, the 100% polar β phase has to be achieved by following mechanical stretching.[21] Ag nanoparticles have also been incorporated in PVDF in *N*,*N*-dimethylformamide (DMF) solvent.[22] The increased polar forms in the nanocomposites have been attributed to the dipolar interaction of the $>CF_2$ dipole with the surface. The influence of carbon nanotubes on PVDF structure has been studied by several groups.[23−29] Lee et al.[29] showed that addition of pristine carbon nanotubes leads to developing β-phase crystal, but the content of β-phase was rather low from the wide-angle X-ray diffraction patterns. Wang et al.[27] reported PVDF/poly(methyl methacrylate) (PMMA)-*g*-MWNT composites using the miscibility between PMMA and PVDF to help disperse the nanotubes in the PVDF matrix. It was found that PMMA-grafted MWCNTs not only were well dispersed in PVDF matrix but also induced formation of β-form PVDF crystallites. Very recently, Mandal et al. prepared PMMA-functionalized MWNTs using nitrene chemistry and fabricated the PVDF nanocomposites by DMF solution blending. Almost full β-form PVDF can be achieved with 5 wt % CNT loadings.[28] Likewise, Manna et al.[29] investigated the PVDF/ester ($-COOC_2H_5$)-functionalized MWCNTs (F-MWCNTs) system and obtained good carbon nanotubes dispersion in PVDF matrix. They found that the F-MWCNTs facilitate conversion of α- to β-form PVDF by the special interaction of the >C═O group in the F-MWCNTs and the $>CF_2$ group. However, only a maximum of 50% β-polymorph PVDF was achieved even with high loading of the F-MWNT in the melt-cooled samples.

In this paper, we first prepared the ionic liquid-modified carbon nanotubes by simply mechanical grinding of the IL with MWCNTs. The IL-MWCNTs are then incorporated into PVDF matrix by the melting blending to fabricate the PVDF/IL-MWCNTs nanocomposites. It was found that IL-MWCNTs can be homogeneously dispersed in the PVDF matrix. More important, the nanocomposites with appropriate content of IL-MWCNTs have 100% polar crystal form when simply cooling down the nanocomposites from the melt state. We found, interestingly, that neither MWCNTs nor IL used independently are effective enough to produce a large content of polar PVDF phases, while only the IL-modified MWCNTs lead to full formation of polar crystal forms at appropriate loading contents. To the best of our knowledge, this is the first time to achieve 100% polar polymorphs in PVDF by melt crystallization without mechanical deformation by nanofillers.

2. EXPERIMENTAL SECTION

2.1. Materials. The poly(vinylidene fluoride) (PVDF) samples were commercially available KF850 (Kureha Chemicals, Japan) . The molecular weight and polydispersity of PVDF, determined by gel permeation chromatography, are M_w = 209 000 and M_w/M_n = 2.0, respectively. Multiwalled carbon nanotubes (MWCNTs), from Showa Denko K. K. (Japan) under the tradename VGCF-X, have a diameter of around 15 nm and length of around 3 μm. The MWCNTs were used as received without further treatment. The ionic liquid (IL), 1-butyl-3-methylimidazolium hexafluorophosphate [BMIM]-$[PF_6]$, was purchased from Aldrich and used as received.

2.2. Sample Preparation. The MWCNTs were first mixed with $[BMIM]^+[PF_6]^-$ using an agate mortar for 15 min at room temperature to prepare IL-modified MWCNTs (designated as IL-MWCNTs). The mass ratio between the IL and the MWCNTs ranges from 0:1 to 5:1. The composites were prepared by direct mixing the obtained IL-MWCNTs with PVDF in a batch mixer (Haake Polylab QC) with a twin screw at a rotation speed of 50 rpm at 190 °C for 5 min. The compositions of the prepared composites are tabulated in Table 1. All samples were designated as P−X−Y, where "X" indicated the mass of MWCNTs and "Y" indicated the mass of IL in the nanocomposites. The IL-MWCNTs were first prepared with the IL to MWCNTs ratio equal to X to Y. After melt mixing, all samples were hot pressed at 200 °C under 14 MPa pressure into films 500 μm thick followed by cool pressing at room temperature. The obtained sheets were directly used for the following characterization.

Table 1. Compositions of the PVDF/IL-MWCNTs Nanocomposites[a]

sample code	PVDF contents (g)	MWCNTs content (g)	IL content (g)
P−0−0	50	0	0
P−0−1	50	0	1
P−1−0	50	1	0
P−1−0.25	50	1	0.25
P−1−0.5	50	1	0.5
P−1−1	50	1	1
P−1−2	50	1	2
P−1−5	50	1	5
P−0.25−0.25	50	0.25	0.25
P−0.5−0.5	50	0.5	0.5

[a]All MWCNTs were first modified with IL and followed by melt compounding with PVDF matrix.

2.3. Characterization. Dispersion of CNTs in the polymer matrix was observed using a field-emission scanning electron microscope (FESEM). A Hitachi S-4800 SEM was used for measurements at an accelerating voltage of 5.0 KV. All samples containing CNTs were fractured by immersion in liquid nitrogen for about 5 min. The fracture surface was then coated with a thin layer of gold before observation.

The crystalline structures of PVDF and composites were studied by Fourier transform infrared spectroscopy (FTIR, Bruker Tensor) instrument and X-ray diffractometry (XRD, Bruker-D8). XRD data were collected from 2θ = 5° to 30° at a scanning speed of 2°/min with a step interval of 0.02°. The instrument was operated at a 35 kV voltage and 30 mA current. FTIR spectra were recorded at a resolution of 2 cm^{-1} and 16 scans from 4000 to 400 cm^{-1}. FTIR measurements were carried

dx.doi.org/10.1021/jp304166t | J. Phys. Chem. B 2012, 116, 8312−8320

out by a transmittance mode, and samples for FTIR were prepared directly by the melt press.

The crystallization and melting behavior of all samples were investigated by means of a differential scanning calorimeter (DSC, TA-Q2000). Before sample scan, the heat flow and temperature of the instrument were calibrated with sapphires and pure indium, respectively. The samples were first heated to 210 °C and held there for 5 min to eliminate previous thermal history. The samples were then cooled to 20 °C, followed by heating again to 210 °C. Both the cooling and the heating rates were 10 °C/min, and the experiments were conducted under a continuous high pure nitrogen atmosphere. The first cooling and second heating traces were recorded.

3. RESULTS

3.1. Dispersion of MWCNTs. Due to the poor compatibility between pristine MWCNTs with polymer matrix, MWCNTs form very dense agglomerates in PVDF matrix, as observed in the SEM image (Figure 1a). In contrast, when IL-modified MWCNTs are used, the compatibility is considerably improved and the MWCNTs are precisely dispersed in the polymer matrix. Most of MWCNTs were found to be embedded in the matrix with the highly exfoliated state. Few MWCNTs domains were also observed with the size of about only several hundred nanometers (Figure 1b). So-called cation−π and/or π−π interactions between the imidazolium cation and the π-electronic nanotubes surface[1−3] can be responsible for the disagglomeration of MWCNTs (as shown the Raman spectroscopy in Figure S1, Supporting Information).

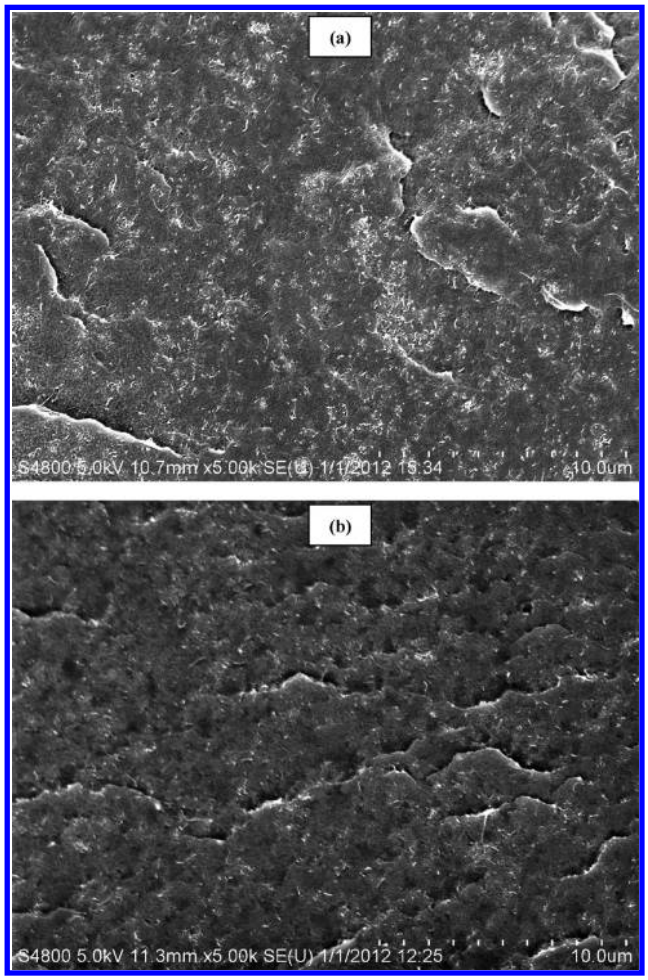

Figure 1. (a) FESEM image of P−1−0, (b) FESEM image of P−1−1.

The improved MWCNTs dispersion by noncovalent functionalization causes an increase of both mechanical properties and electrical conductivity. Elongation at the break of the sample with the IL-modified MWCNTs is much higher than that of the sample with pristine MWCNTs. Moreover, the IL-modified MWCNTs exhibit drastically different effects on the electrical conductivity of the nanocomposites. Detailed physical properties of the prepared nanocomposites will be reported elsewhere.

3.2. IL-MWCNTs Impact on the Crystallization Behavior of PVDF. FTIR has been widely used to determine the crystal forms of PVDF. Fortunately, there is no absorption band of the used ionic liquid overlapped with the characteristic crystal bands of PVDF except for 840 cm^{-1}. Figure 2 shows the FTIR spectra of neat PVDF (P−0−0), PVDF with only IL (P−0−1), PVDF with only MWCNTs (P−1−0), and PVDF/IL-MWCNTs (P−1−1). According to the literature,[14,15] the peaks at 408, 532, 615, 764, 796, 855, 976, and 1385 cm^{-1} are the characteristic absorption peaks for α-phase identification. The polar crystalline phases show characteristic absorptions at 445

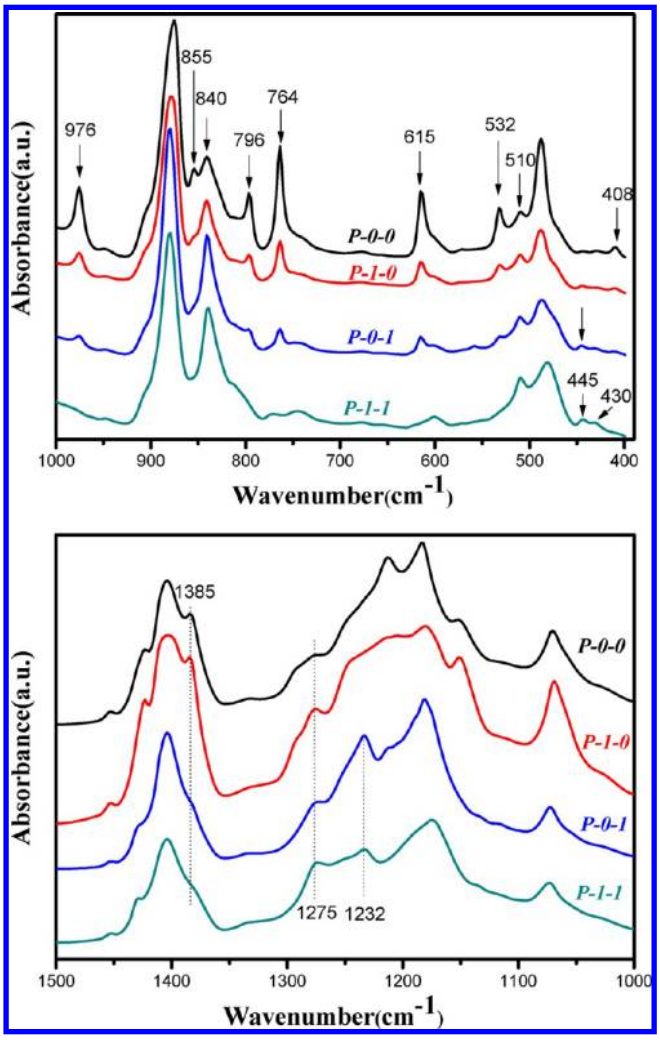

Figure 2. FTIR spectra of neat PVDF (P−0−0), PVDF/MWCNTs (P−1−0), PVDF/IL (P−0−1), and PVDF/IL-MWCNTs (P−1−1).

dx.doi.org/10.1021/jp304166t | J. Phys. Chem. B 2012, 116, 8312−8320

and 1275 cm^{-1} for the β-phase and at 430 and 1232 cm^{-1} for the γ-phase.[30−32] Both β- and γ-phases show the absorption at 510 cm^{-1}. The fact that strong absorption peaks at 408, 532, 615, 764, 796, 855, and 976 cm^{-1} and weak absorption peak at 1385 cm^{-1} are observed in FTIR spectra of the neat PVDF (P−0−0) indicates that the crystals in neat PVDF are mainly the nonpolar α-phase. However, very weak peaks at 445, 510, and 840 cm^{-1} can also be observed, which means that trace amounts of polar β phase are also present in neat PVDF. The fraction of the polar crystal form in a sample containing both forms can be calculated by assuming that IR absorption follows the Lambert−Beer law[33]

$$F(p) = A_p/(1.26A_n + A_p) \quad (1)$$

where A_n and A_p are the absorbance intensities at 764 (representing nonpolar α-phase) and 510 cm^{-1} (representing polar phase), respectively. Note that the calculated F is the total content of polar β and γ phases because the absorption at 510 cm^{-1} was used in eq 1. The calculated polar form content is listed in Table 2. Only 1.9% polar crystals are formed in neat PVDF. For the P−1−0 sample, the polar crystal content was calculated to be 6.1%, which is higher than that for neat PVDF, indicating the slight enhancement of polar crystals form by the pristine MWCNTs. The fact that the γ-peak at 1232 cm^{-1} was not observed for both P−0−0 and P−1−0 samples indicates that there are no γ-crystals in these two samples. In fact, a small amount of β-phase induced by MWCNTs has been reported previously.[26,27] Significantly more polar crystal forms are seen in the P−0−1 sample (PVDF/IL blend), as shown in Figure 2, the characteristic absorption peaks for polar crystal forms at 445, 510, and 840 cm^{-1} become clearly observable. The calculated polar-form content increases to 23%. The results indicate that the IL is more effective to induce formation of polar crystal forms than pristine MWCNTs. Note that some γ-crystals exist in the P−0−1 sample because of the observed γ-peak at 1232 cm^{-1}. Surprisingly, when the IL-modified MWCNTs were incorporated into the PVDF sample, no α-form absorption was seen and only the absorption peaks for polar crystal forms can be observed in Figure 2. This means that the IL-MWCNTs induce the 100% polar crystal forms of PVDF in the nanocomposites when simply cooled down from the melt. For the P−1−1 sample with full polar phases, we also observe some content of γ crystals. The relative contents for the polar β and γ forms will be discussed in section 3.5.

Table 2. Impact of IL and MWCNTs on the melting and crystallization of PVDF

sample	P−0−0	P−1−0	P−0−1	P−1−1
polar-phase content (%)	1.9	6.1	23	100
T_c (°C)	141.5	151.4	139.2	154.9
T_m (°C)	172	174.0	179.4	180.2

X-ray diffraction presents the direct characterization of the PVDF crystal forms. Figure 3 shows the X-ray diffraction patterns of the corresponding samples in Figure 2. Four characteristic diffraction peaks were observed at 17.7°, 18.4°, 20.0°, and 26.6° for neat PVDF, which are assigned to (100), (020), (110), and (021) reflections of α-phase crystal,[14] indicating the very high α-crystal forms content in the melt-crystallized PVDF. For the P−1−0 sample, all α characteristic diffraction peaks are still observed but with a small shoulder at 2θ = 20.3°, the characteristic diffraction of polar β- and/or γ-phase.[35,36] This means that incorporation of pristine MWCNTs induces formation of a very small amount of polar phases. The relative intensity of the characteristic polar peak at 20.3° is stronger for the P−0−1 sample compared to the P−1−0 one because the increased polar crystal forms upon addition of IL. One can see that a considerable α form still exists in P−0−1. In contrast, no diffraction peaks of α crystals were seen in the XRD pattern of P−1−1, indicating 100% polar crystal forms in this sample. The WAXD results are highly consistent with the FTIR results in Figure 2.

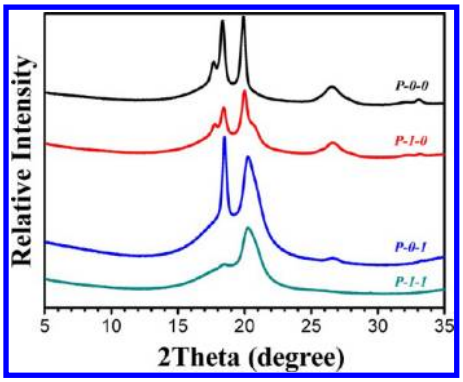

Figure 3. XRD patterns of neat PVDF (P−0−0), PVDF/MWCNTs (P−1−0), PVDF/IL (P−0−1), and PVDF/IL-MWCNTs (P−1−1).

It has been reported that the melting temperature of the α-phase is lower than that of the polar β- and γ-phases for PVDF.[37,38] Figure 4a illustrates the second DSC heating curves of pure PVDF and its compounds with MWCNTs, ILs, and IL-MWCNTs. It is apparent from Figure 4a that the pure PVDF and P−1−0 exhibit a melting peak at about 173 °C with a

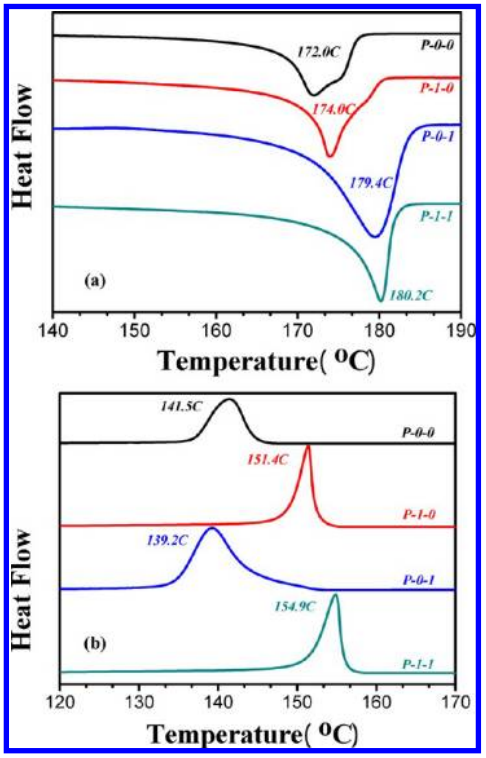

Figure 4. DSC heating (a) and cooling (b) curves of neat PVDF (P−0−0), PVDF/MWCNTs (P−1−0), PVDF/IL (P−0−1), and PVDF/IL-MWCNTs (P−1−1).

dx.doi.org/10.1021/jp304166t | J. Phys. Chem. B 2012, 116, 8312−8320

shoulder at higher temperature region. Such melting behavior arises due to melt recrystallization of α crystals.[39,40] The P−0−1 sample contains more polar (β and γ forms) crystals that melt at higher temperature. However, the fact that the endothermic peak of the P−0−1 sample is rather wide indicates the melting contribution of both nonpolar α and polar crystals in the sample, as shown in the results of FTIR and WAXD. For the P−1−1 sample, only one narrow melting peak at 180.2 °C can be observed, suggesting that the sample is becoming a polar phase with higher melting temperature, in agreement with XRD and FTIR results.

First DSC cooling thermograms from the melt of the corresponding samples are shown in Figure 4 (b). The melt crystallization temperature of neat PVDF is located at 141.5 °C. The crystallization temperature shifted to 151.4 °C when 2 phr pristine MWCNTs were incorporated into the PVDF. This means that the pristine MWCNTs take the role as the nucleation agent for PVDF and accelerate crystallization of PVDF. Such effects have also been reported in previous literature.[41,42] In contrast, the melt crystallization peak temperature of the PVDF/IL blends (P−0−1) is 139.2 °C, which is lower than that of neat PVDF. This can be attributed to the miscibility between the IL and PVDF. The used IL is fully miscible with PVDF, as indicated by the significantly shifting T_g of PVDF for the PVDF/IL blends (Figure S2, Supporting Information). The small IL molecules impede the crystallization of PVDF and consequently decrease the crystallization temperature of PVDF. For the P−1−1 sample where IL-MWCNTs were used, the melt crystallization temperature is 154.9 °C, which is even higher than the P−1−0 sample. This means that the IL-MWCNTs with a ratio of 1:1 are more efficient as a nucleation agent for the PVDF than pristine MWCNTs.

3.3. IL to MWCNTs Ratio Effects on the Crystallization of PVDF. It is shown that incorporation of IL-modified MWCNTs (1:1) into the PVDF matrix not only accelerates crystallization of PVDF but also induces full polar crystals simply crystallized from the melt state. It is therefore important to investigate the IL to MWCNTs ratio effects on the crystallization behavior of PVDF. We conducted the experiments by varying the IL contents during the surface modifying of MWCNTs while keeping the constant MWCNTs loadings in the nanocomposites. The FTIR spectra and calculated polar form contents as a function of the IL to MWCNT ratio are shown in Figure 5. A small amount of IL enhances formation of polar crystals drastically. However, the 100% polar crystal form can only be achieved when the IL to MWCNTs ratio is higher than 1. The XRD results are also consistent with those in FTIR (Figure S3, Supporting Information). The MWCNTs modified with a small amount of IL (P−1−0.25 and P−1−0.5 samples) cannot make the samples with 100% polar crystal phases, as indicated in the shoulder diffraction in the 2θ range of 14−19° in XRD profiles.

The crystallization temperature (T_c) and melting temperature (T_m) of the PVDF crystals as a function of the IL to CNTs ratio from the DSC curves are shown in Figure 6. We have shown that the pristine MWCNTs accelerate the PVDF crystallization rate in Figure 4. P−1−0.25 and P−1−0.5 have the same crystallization temperature at 155.3 °C, which is 3.9 °C higher than 151.4 °C, the T_c of P−1−0. This means that the modified MWCNTs using a small amount of IL have more efficient nucleation effects than the pristine MWCNTs. The nucleation synergetic effects by IL and MWCNTs can be

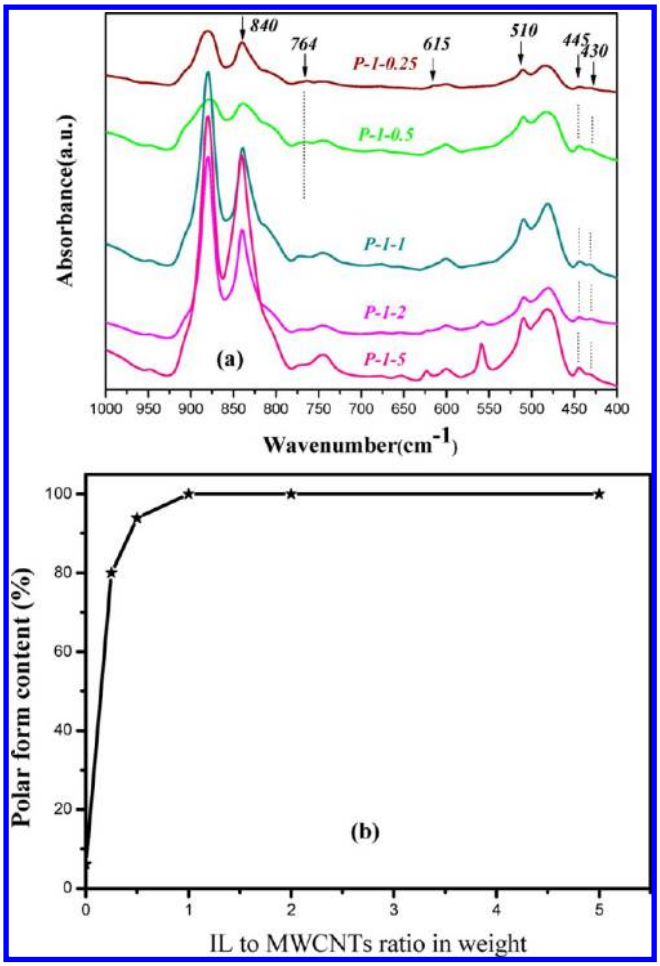

Figure 5. (a) FTIR spectra of PVDF/IL-MWCNTs nanocomposites with various IL to MWCNTs ratios in weight, and (b) calculated polar-phase content (wt %) as a function of the IL to MWCNTs ratio.

attributed to the specific interaction between the PVDF molecular chains with the imidazolium cations wrapped on the surface of MWCNTs. Such interaction speeds up formation of oriented zigzag conformation of PVDF chains, thus accelerating crystallization of PVDF. However, the overloading of IL results in the saturation of the MWCNTs surface modification and the free IL decreases the crystallization temperature of PVDF because of its miscibility with PVDF. Therefore, the T_c of PVDF nanocomposites decreases with increasing IL to MWCNTs ratio over 1:1. The melting temperatures of the formed crystals were also very dependent on the IL to MWCNTs ratio. A small amount of IL-MWCNTs abruptly increased the melting temperature because of the high content in the polar PVDF forms in P−1−0.25. When increasing the IL to MWCNTs ratio in the range from 1:1 to 5:1 the polar form content keeps almost no change but the melting temperature decreases. Depression of T_m of the polar crystals may be due to the specific interactions between the free IL molecules with PVDF. The phenomenon has been widely observed for many miscible crystalline/amorphous polymer blends.[43] One should note that the maximum T_c and T_m is not occurring just at the 1:1 ratio of IL and MWCNTs where 100% polar phase was obtained. The reason is not clear, but it may be related not only to the crystal phase but also to the MWCNTs dispersion state in PVDF matrix. On one hand, the IL-MWCNTs facilitate crystallization of PVDF into polar phase

dx.doi.org/10.1021/jp304166t | J. Phys. Chem. B 2012, 116, 8312−8320

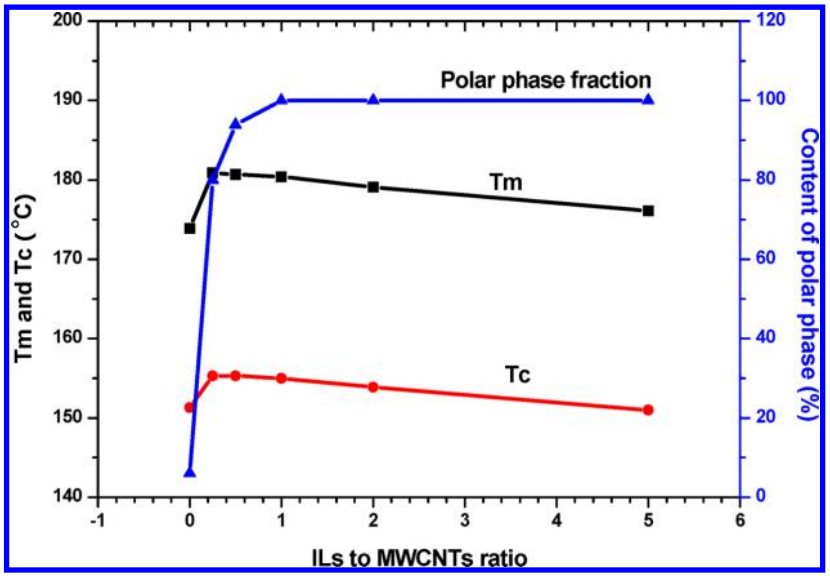

Figure 6. Crystallization temperature (T_c) and melting temperature (T_m) of PVDF in the nanocomposites as a function of the IL to MWCNTs ratio.

with a high melting temperature. On the other hand, PVDF crystal growth is confined by the improved dispersion of MWCNTs, which induces \ imperfect crystals with a lower melting temperature.

3.4. IL-MWCNTs Loading Effects on Crystallization of PVDF. It has been shown that the maximum polar crystal forms and the highest nucleation effects can be obtained when the ILs to MWCNTs ratio is about 1. In this section, we investigate the IL-MWCNTs loading effects on the crystallization of PVDF while keeping the IL to MWCNTs ratio of 1. It was found that the polar crystal form content increases with increasing IL-MWCNTs loading contents. The characteristic absorption peaks for the α-form were clearly observed for the P−0.25−0.25 and P−0.5−0.5 samples (Figure S4, Supporting Information), while only polar crystal forms exist in the P−1−1 sample. It is considered that the high content of MWCNTs loading provides sufficient CNT surface area to nucleate the PVDF chains; thus, more polar PVDF crystals are obtained. For the samples with a low IL-MWCNTs loading concentration, partial nucleation in the α-form for the PVDF chains far from the MWCNTs surface occurs, which leads to formation of a mixture of nanopolar α and polar polymorphs in the composites. Such phenomena can be confirmed by the lower crystallization temperature for the P−0.25−0.25 sample than that for P−1−1 in Figure 7.

3.5. Polar β- and γ-Phases in the Nanocomposites. The β- and γ-phases have very similar X-ray diffraction patterns, and many FTIR absorptions are also overlapped together, so it is important to elucidate whether the prepared nanocomposites contain γ phase. Figure 8a shows FTIR spectra for the nanocomposites with various IL to MWCNTs ratios in the wavenumber range of 1500−1000 cm^{-1}. It is clear that both the characteristic β absorption at 1275 cm^{-1} and the characteristic γ absorption at 1232 cm^{-1} are observed, indicating that the polar crystal phases in the nanocomposites are in fact the mixture of β and γ forms. Unfortunately, it is difficult to calculate the ratio of the two crystal forms. However, it is seen that from Figure 8b that the intensity of the 1232 cm^{-1} peak decreases and that of the 1275 cm^{-1} peak increases with increasing the IL to WMCNTs ratio, indicating the IL facilitates formation of the β-crystal form.

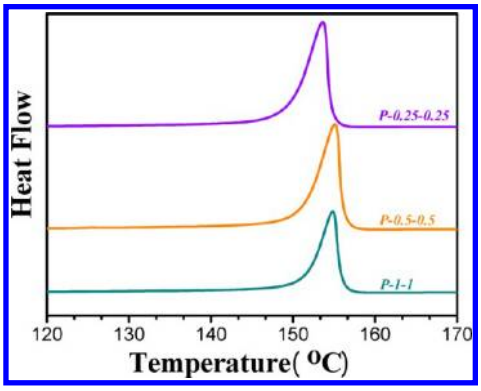

Figure 7. DSC cooling curves of the PVDF/IL-MWCNTs nanocomposites with various amounts of MWCNTs loading while keeping the IL to MWCNTs ratio of 1.

4. DISCUSSION

It is well documented that the imidazolium ions of ILs could be adsorbed onto the π-electronic surface of the nanotubes through possible cation−π interactions.[1−3] In the present system, the D and G bands of pristine MWNTs at 1303 and 1579 cm^{-1} were observed to shift to 1304.5 and 1598 cm^{-1}, respectively, for IL-MWNTs (2:1) in Figure S1, Supporting Information. A red shift in both the D and the G bands indicates a clear interaction between the IL and MWNTs, which has been suggested to be the so-called "cation−π" and/or π−π interaction between the cationic ions and the π-electronic nanotube surface. On the other hand, we found that the used ionic liquid is fully miscible with PVDF, which may be attributed to the specific interaction between imidazolium ions with $>CF_2$. Such interaction can be confirmed using the FTIR spectra shown in Figure 9. The amorphous peak of CF_2−CH_2 bending vibration (875 cm^{-1})[44] in neat PVDF (sample P−0−0) shifts to a higher energy region (879 cm^{-1}), indicating these $>CF_2$ groups in the PVDF chains are interacting with the imidazolium ring in IL. At the same time, the imidazolium ring absorption at 1171 cm^{-1}[145] for neat IL shifts to 1180 cm^{-1} after compounding with PVDF in P−0−1. Therefore, the IL takes the role as a linker to improve the compatibility between MWCNTs and PVDF matrix. The MWCNTs can be

dx.doi.org/10.1021/jp304166t | J. Phys. Chem. B 2012, 116, 8312−8320

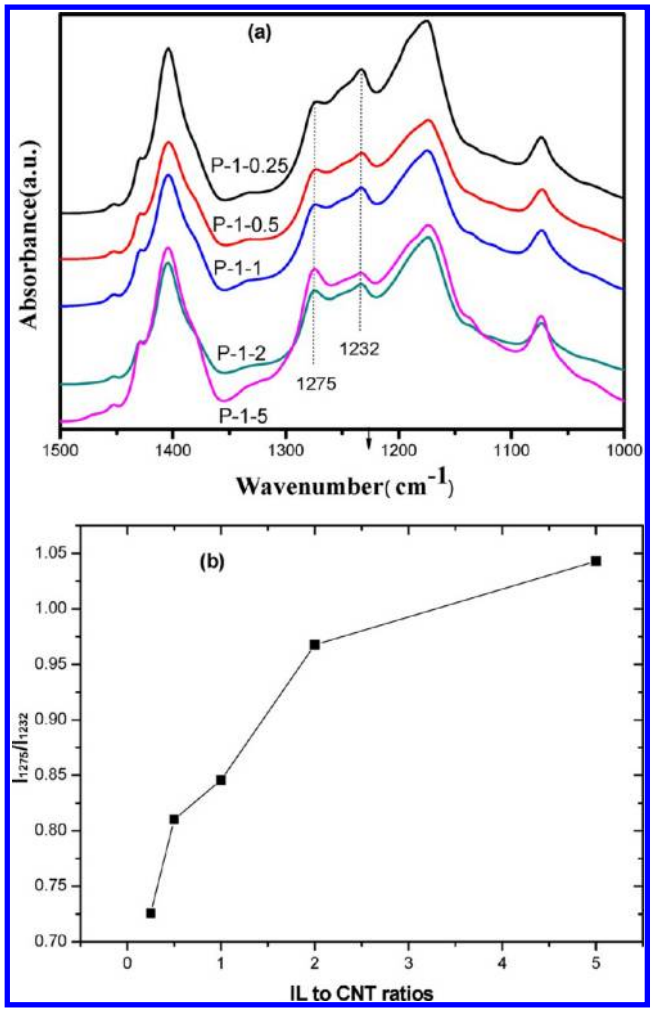

Figure 8. (a) FTIR spectra of PVDF/IL-MWCNTs nanocomposites with various IL to MWCNTs ratios in the wavenumber range of 1500−1000 cm^{-1}, and (b) intensity ratio of charancteristic β form and γ form (I_{1275}/I_{1232}) as a function of the IL to CNT ratios.

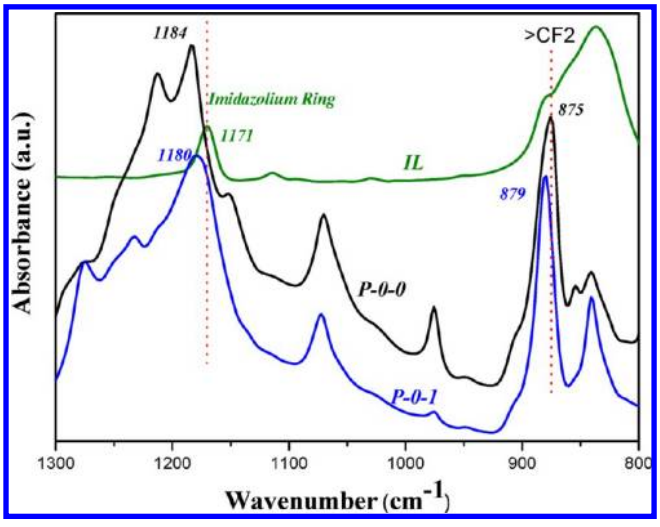

Figure 9. FTIR spectra of the neat IL, neat PVDF (P−0−0), and PVDF/IL (P−0−1).

homogeneously dispersed in the PVDF matrix by melt compounding after grinding with the ionic liquids.

Nandi et al. also reported the 100% β-phase of PVDF in the nanocomposites using PMMA-*g*-graphene and ester-*g*-MWCNTs as the nanofillers.[28,29,35] However, they showed that full β form can only be achieved by solution crystallization from DMF, and only a maximum 50% of β-phase was obtained for the melt-cooled nanocomposites. In the present work, we displayed that incorporation of IL-MWCNTs induces significantly enhanced β- and γ-form content and 100% polar crystal form can be easily achieved by simply cooling the nanocomposites from the melt state. The surface of pristine MWCNTs has zigzag carbon atoms, which may match in part the all-trans conformation of PVDF in the melt state; thus, the pristine MWCNTs has a nucleating effect and induces partial β crystals (the content is 6.1%). However, the MWCNTs surface modification by the ionic liquid significantly enhances both the nucleating effects and the crystals form transitions. As schematically drawn in Figure 10, the cation−π

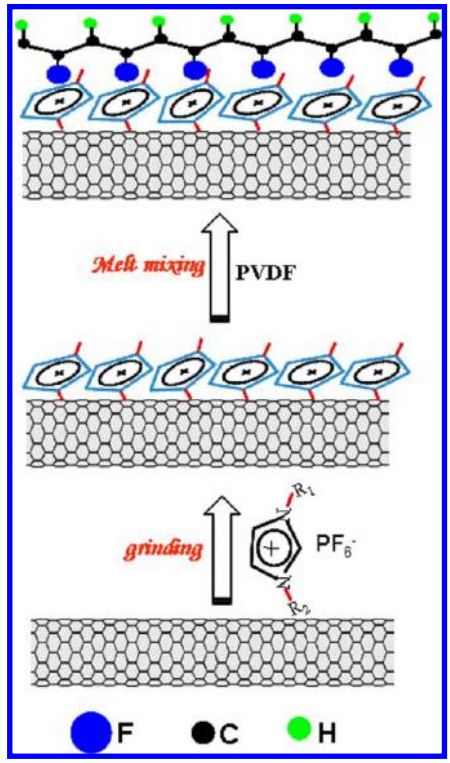

Figure 10. Schematic diagram of the linker effect of IL for PVDF and MWCNTs as well as the mechanism for formation of PVDF TT conformations.

interactions between the ionic liquids and the carbon nanotubes induce the imidazolium cation rings parallel to the conjugated rings of the carbon nanotubes. The specific interaction between the imidazolium cation with $>CF_2$ (as shown in Figure 9) renders the $>CF_2$ located along the one side of the molecular chain. Therefore, PVDF chains adopted the all-trans conformation (or TTTG conformations) on the surface of IL-coated MWCNTs. Once the polar β or γ nuclei formed on the MWCNTs surface, rapid crystallization occurs due to high nucleation density and consequently polar polymorphs are produced for the melt-crystallized nanocomposites. In addition, dispersion of MWCNTs is significantly improved when MWCNTs are modified by IL, which leads to the drastically increased polar form nucleation site, which also contributes to the full polar phase during melt crystallization.

dx.doi.org/10.1021/jp304166t | J. Phys. Chem. B 2012, 116, 8312−8320

Yu et al.[46] compared the adsorption energy for the α and β polymorph of PVDF on the surface of carbon nanotube and concluded that the adsorption energy for the β polymorph is higher than the α form. Therefore, a large amount of energy is required for transforming trans−gauche−trans−gauche (TGTG′) into trans−trans (TT) conformations. This is the reason that only few percent of β-form was observed when pristine MWCNTs were used. However, the specific interaction between $>CF_2$ with imidazolium cations can overcome such energy barrier between the α polymorph and the β polymorph, and a large amount of β crystals can be achieved when the IL-coated MWCNTs were added. The functions of the anions in the nanocomposites should be noted. It has been reported that an extended network of cations and anions connected together by hydrogen bonds in 1,3-dialkylimidazolium salts exists.[47] Therefore, PF_6 anions do not affect formation of the zigzag conformation of PVDF in this work because the interaction between $>CF_2$ with imidazolium cations is vertical to the imidazolium ring plane.

The above analysis indicates that the ordered arrangement of the imidazolium ring on the surface of MWCNTs is critically important for making β nuclei. In other words, the first treatment of MWCNTs by the grinding of IL may benefit formation of the IL wrapping on the surface of MWCNTs, thus benefiting formation of the β crystal form. To prove such hypothesis, we conducted another experiment using the same composition with the sample of P−1−1 but simultaneously (one step) mixing PVDF, pristine MWCNTs, and the IL at the same melt mixing conditions. FTIR spectroscopy of the obtained sample has been compared with that of P−1−1, as shown in Figure 11. The characteristic α phase at 615 and 764 cm^{-1} can be clearly observed for the one-step-mixed sample, and the polar phase content is about 80%, which is lower than the content in P−1−1 sample. We considered that few IL molecules are coated on the surface of MWCNTs for the simultaneously mixed sample, which induced deceased polar phase content in the sample.

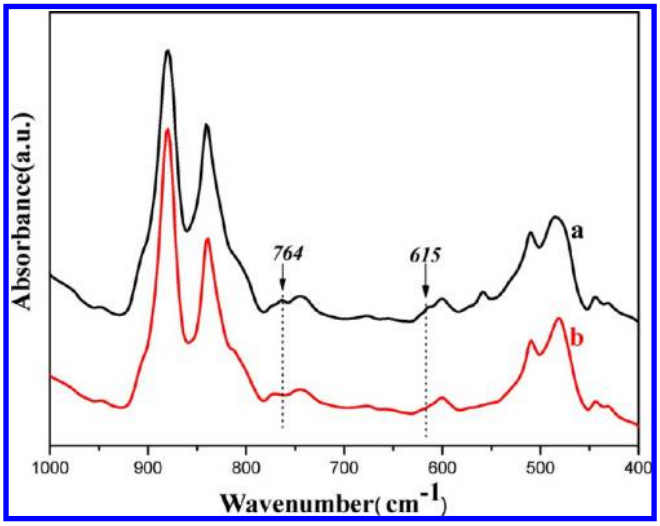

Figure 11. Comparison of FTIR spectroscopy of (a) one-step-mixed nanocomposites and (b) nanocomposites using IL-MWCNTs as the fillers.

The MWCNTs surface coated by the ionic liquid molecules exhibits more efficient nucleation effects for PVDF than the pristine MWNTs, which can also be attributed to the specific interaction between well-arranged imidazolium cation with the $>CF_2$ of PVDF. The TT conformations are absorbed on the surfaces of MWCNTs to form the large amount of β nuclei; subsequently, the crystals grow from these nuclei. However, the overloading of ILs results in saturation of the MWCNTs surface modification and the free ILs decrease the crystal growth rate of PVDF. Therefore, the decreased crystallization rate was observed for the P−1−2 and P−1−5 samples.

5. CONCLUSIONS

We succeeded in fabricating PVDF nanocomposites with full polar crystal form using ionic liquid-modified carbon nanotubes as the filler. The 100% polar phase was simply achieved by melt crystallization without mechanical deformation. We found that IL not only helps to disperse the carbon nanotubes in the PVDF matrix but also causes the PVDF chains to adopt the all trans (TTTT) conformations that lead to formation of polar PVDF crystals. DSC study shows that the IL-modified MWCNTs have more efficient nucleating effects for PVDF crystallization than the pristine MWCNTs. Both formation of high content polar crystal forms and the nucleation effects by the IL-MWCNTs have been attributed to the specific interactions of the IL with MWCNTs and the IL with $>CF_2$ groups in PVDF chains, resulting in the regular $>CF_2$ arrangement on the MWCNTs surface with all zigzag conformations.

■ ASSOCIATED CONTENT

Supporting Information

Raman spectra, DMA results for PVDF/IL blends, and XRD patterns and FTIR spectra. This material is available free of charge via the Internet at http://pubs.acs.org.

■ AUTHOR INFORMATION

Corresponding Author

*Phone: 86-571-2886-6579. Fax: 86-571-2886-7899. E-mail: yongjin-li@hznu.edu.cn.

Notes

The authors declare no competing financial interest.

■ ACKNOWLEDGMENTS

This work was financially supported by the National Natural Science Foundation of China (21074029, 21104014, 51173036, 21104013) and Zhejiang Provincial Natural Science Foundation of China (R4110021). This work was also partially supported by the Project of Zhejiang Key Scientific and Technological Innovation Team No.2010R50017.

■ REFERENCES

(1) Fukushima, T.; Kosaka, A.; Ishimura, Y.; Yamamoto, T.; Takigawa, T.; Ishii, N.; Aida, T. *Science* **2003**, *300*, 2072.
(2) Bellayer, S.; Gilman, J. W.; Eidelman, N.; Bourbigot, S.; Flambard, X.; Fox, D. M.; Delong, H. C.; Trulove, P. C. *Adv. Funct. Mater.* **2005**, *15*, 910.
(3) Fukushima, T.; Kosaka, A.; Yamamoto, Y.; Aimiya, T.; Notazawa, S.; Takigawa, T.; Inabe, T.; Aida, T. *Small* **2006**, *2*, 554.
(4) Shang, S. M.; Zeng, W.; Tao, X. M. *J. Mater. Chem.* **2011**, *21*, 7274.
(5) Carrion, F. J.; Espejo, C.; Sanes, J.; Bermudez, M. D. *Compos. Sci. Technol.* **2010**, *70*, 2160.
(6) Le Bideau, J.; Viau, L.; Vioux, A. *Chem. Soc. Rev.* **2011**, *40*, 907.
(7) Zhao, L.; Li, Y.; Cao, X.; You, J.; Dong, W. *Nanotechnology* **2012**, *23*, 255702.

(8) Lang, S. B.; Muensit, S. *Appl. Phys. A: Mater. Sci. Process.* **2006**, *85*, 125.
(9) Mohammadi, B.; Yousefi, A. A.; Bellah, S. M. *Polym. Test.* **2007**, *26*, 42.
(10) Salimi, A.; Yousefi, A. A. *Polym. Test.* **2003**, *22*, 699.
(11) Hattori, T.; Kanaoka, M.; Ohigashi, H. *J. Appl. Phys.* **1996**, *79*, 2016.
(12) David, L.; Winsor, J. I.; Scheinbeim, B. A. *J. Polym. Sci., Part B* **1996**, *34*, 2967.
(13) Branciforti, M. C.; Sencadas, V.; Lanceros-mendez, S.; Gregorio, R. *J. Polym. Sci., Part B: Polym. Phys.* **2007**, *45*, 2793.
(14) Gregorio, R. *J. Appl. Polym. Sci.* **2006**, *100*, 3272.
(15) Yee, W. A.; Kotaki, M.; Liu, Y.; Lu, X. H. *Polymer* **2007**, *48*, 512.
(16) Yu, W. X.; Zhao, Z. D.; Zheng, W. T.; Long, B. H.; Jiang, Q.; Li, G. W. *Polym. Eng. Sci.* **2009**, *49*, 492.
(17) Patro, T. U.; Mhalgi, M. V.; Khakhar, D. V.; Misra, A. *Polymer* **2008**, *49*, 3486.
(18) Dillon, D. R.; Tenneti, K. K.; Li, C. Y.; Ko, F. K.; Sics, I. S.; Hsiao, B. S. *Polymer* **2006**, *47*, 1678.
(19) Buckley, J.; Cebe, P.; Cherdack, D.; Crawford, J.; Ince, B. S.; Jenkins, M.; Pan, J. J.; Reveley, M.; Washington, N.; Wolchover, N. *Polymer* **2006**, *47*, 2411.
(20) Pramoda, K. P.; Mohamed, A.; Phang, I. Y.; Liu, T. X. *Polym. Int.* **2005**, *54*, 226.
(21) Sadeghi, F.; Ajji, A. *Polym. Eng. Sci.* **2009**, *49*, 200.
(22) Manna, S.; Batabyal, S. K.; Nandi, A. K. *J. Phys. Chem. B* **2006**, *110*, 12318−12326.
(23) Levi, N.; Czerw, R.; Xing, S. Y.; Iyer, P.; Canroll, D. L. *Nano Lett.* **2004**, *4*, 1267.
(24) He, L. H.; Sun, J.; Zheng, X. L.; Xu, Q.; Song, R. *J. Appl. Polym. Sci.* **2011**, *119*, 1905.
(25) He, L. H.; Xu, Q.; Hua, C. W.; Song, R. *Polym. Comp.* **2010**, *43*, 134.
(26) Lee, J. S.; Kim, G. H.; Kim, W. W.; Oh, K. H.; Kim, H. T.; Hwang, S. S.; Hong, S. M. *Mol. Cryst. Liq. Cryst.* **2008**, *491*, 247.
(27) Wang, M.; Shi, J. H.; Pramoda, K. P.; Goh, S. H. *Nanotechnology* **2007**, *18*, 235701.
(28) Mandal, A.; Nandi, A. K. *J. Mater. Chem.* **2011**, *21*, 15752.
(29) Manna, S.; Nandi, A. K. *J. Phys. Chem. C* . **2007**, *111*, 14670.
(30) Gregorio, R.; Cestari, M. *J. Polym. Sci. Polym. Phys.* **1994**, *32*, 859.
(31) Kim, K. J.; Cho, Y. J.; Kim, Y. H. *Vib. Spectrosc.* **1995**, *9*, 147.
(32) Ince-Gundz, S.; Alpern, R. A.; Amarer, D.; Crawford, J.; Dolan, B.; Kobylarz, R; Raveley, M.; Cebe, P. *Polymer* **2010**, *51*, 1485.
(33) Salimi, A.; Yousefi, A. A. *J. Polym. Sci., Part B: Polym. Phys.* **2004**, *42*, 3487.
(34) Nam, Y. W.; Kim, W. N.; Cho, Y. H.; Chae, D. W.; Kim, G. H.; Hong, S. P.; Hwang, S. S.; Hong, S. M. *Macromol. Symp.* **2007**, *249*−*250*, 478.
(35) Layek, R. K.; Samanta, S.; Chatterjee, D. P.; Nandi, A. K. *Polymer* **2010**, *51*, 5846.
(36) Huang, X. Y.; Jiang, P. K.; Kim, C.; Liu, F.; Yin, Y. *Eur. Polym. J.* **2009**, *45*, 377.
(37) Andrew, J. S.; Clarke, D. R. *Langmuir* **2008**, *24*, 670.
(38) Sadeghi, F.; Ajji, A. *Polym. Eng. Sci.* **2009**, 201.
(39) Nandi, A. K.; Mandelkern, L. *J. Polym. Sci., Part B: Polym. Phys.* **1991**, *29*, 1287.
(40) Prest, W. M.; Luca, D. J. *J. Appl. Phys.* **1975**, *46*, 4138.
(41) Vidhate, S.; Shaito, A.; Chung, J.; D'Souza, N. A. *J. Appl. Polym. Sci.* **2009**, *112*, 254.
(42) Huang, W. W.; Edenzon, K.; Fernandez, L.; Razmpour, S.; Woodburn, J.; Cebe, P. *J. Appl. Polym. Sci* . **2010**, *115*, 3238.
(43) Nishi, T.; Wang, T. T. *Macromolecules* **1975**, *8*, 909.
(44) Enomoto, S.; Kawai, Y.; Sugita, M. *J. Polym. Sci., Part A-2* **1968**, *6*, 861.
(45) Sergey, A. K; Elena, E. Z.; Ana, V.; Paul, J. D. *J. Phys. Chem. A* **2007**, *111*, 352−370.
(46) Yu, S. S.; Zheng, W. T.; Yu, W. X.; Zhang, Y. J.; Jiang, Q.; Zhao, Z. D. *Macromolecules* **2009**, *42*, 8870.
(47) Dupont, J. *J. Braz. Chem. Soc.* **2004**, *15*, 341.